AD-A156 916 DYNAMICS OF IMPLODING NEON GAS PUFF PLASMAS I(U) NAVAL RESEARCH LAB WASHINGTON DC R W CLARK ET AL. 19 JUL 85 NRL-MR-5613 1/1

UNCLASSIFIED F/G 20/9 NL

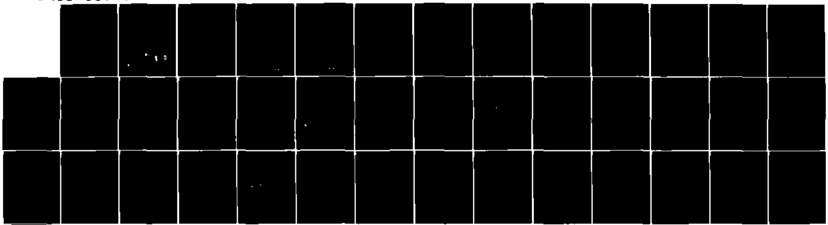

END
DATE
FILMED
8-85

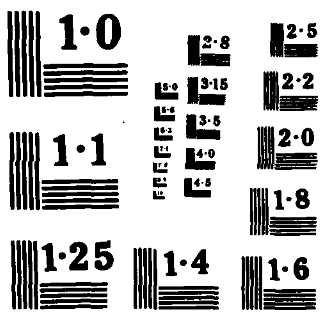
1·0
2·8
2·5
3·15
2·2
3·5
2·0
1·1
4·0
4·5
1·8
1·25
1·4
1·6

2

NRL Memorandum Report 5613

AD-A156 916

Dynamics of Imploding Neon Gas Puff Plasmas — I

R. W. CLARK AND J. DAVIS

Plasma Radiation Branch
Plasma Physics Division

July 19, 1985

This research was sponsored by the Defense Nuclear Agency under Subtask T99QMXLA, work unit 00004 and work unit title "Advanced Simulation Concepts,"

NAVAL RESEARCH LABORATORY
Washington, D.C.

SECURITY CLASSIFICATION OF THIS PAGE

REPORT DOCUMENTATION PAGE

1a. REPORT SECURITY CLASSIFICATION: UNCLASSIFIED

1b. RESTRICTIVE MARKINGS:

2a. SECURITY CLASSIFICATION AUTHORITY:

2b. DECLASSIFICATION / DOWNGRADING SCHEDULE:

3. DISTRIBUTION / AVAILABILITY OF REPORT: Approved for public release; distribution unlimited.

4. PERFORMING ORGANIZATION REPORT NUMBER(S): NRL Memorandum Report 5613

5. MONITORING ORGANIZATION REPORT NUMBER(S):

6a. NAME OF PERFORMING ORGANIZATION: Naval Research Laboratory

6b. OFFICE SYMBOL (If applicable): Code 4720

7a. NAME OF MONITORING ORGANIZATION: Defense Nuclear Agency

6c. ADDRESS (City, State, and ZIP Code): Washington, DC 20375-5000

7b. ADDRESS (City, State, and ZIP Code): Washington, DC 20305

8a. NAME OF FUNDING / SPONSORING ORGANIZATION: Defense Nuclear Agency

8b. OFFICE SYMBOL (If applicable): RAEV

9. PROCUREMENT INSTRUMENT IDENTIFICATION NUMBER:

8c. ADDRESS (City, State, and ZIP Code): Washington, DC 20305

10. SOURCE OF FUNDING NUMBERS

PROGRAM ELEMENT NO.	PROJECT NO.	TASK NO.	WORK UNIT ACCESSION NO.
62715H	85-579		DN880-191

11. TITLE (Include Security Classification): Dynamics of Imploding Neon Gas Puff Plasmas — I

12. PERSONAL AUTHOR(S): Clark, R.W. and Davis, J.

13a. TYPE OF REPORT: Interim

13b. TIME COVERED: FROM 10/84 TO 10/85

14. DATE OF REPORT (Year, Month, Day): 1985 July 19

15. PAGE COUNT: 41

16. SUPPLEMENTARY NOTATION: This research was sponsored by the Defense Nuclear Agency under Subtask T99QMXLA, work unit 00004 and work unit title "Advanced Simulation Concepts."

17. COSATI CODES

FIELD	GROUP	SUB-GROUP

18. SUBJECT TERMS (Continue on reverse if necessary and identify by block number): Gas puff, Neon, Dynamics, Radiation

19. ABSTRACT (Continue on reverse if necessary and identify by block number)

The implosion of a cylindrical neon puff-gas plasma on a low density central core is investigated using a 1D non-LTE radiation-hydrodynamic model. Radiation transports energy into the core plasma and produces heating deep within the puff-gas. The implosion very efficiently converts kinetic energy into soft x-rays; about two-thirds of the initial plasma energy is radiated away. Comparison is made with a neon puff-gas implosion without a central core and with pure hydrodynamic calculations. For each case, detailed self-consistent emission spectra and energy partitioning are discussed.

20. DISTRIBUTION / AVAILABILITY OF ABSTRACT: ☒ UNCLASSIFIED/UNLIMITED ☐ SAME AS RPT ☐ DTIC USERS

21. ABSTRACT SECURITY CLASSIFICATION: UNCLASSIFIED

22a. NAME OF RESPONSIBLE INDIVIDUAL: Jack Davis

22b. TELEPHONE (Include Area Code): (202) 767-3278

22c. OFFICE SYMBOL: Code 4720

DD FORM 1473, 84 MAR — 83 APR edition may be used until exhausted. All other editions are obsolete.

SECURITY CLASSIFICATION OF THIS PAGE

CONTENTS

DYNAMICS OF IMPLODING NEON GAS PUFF PLASMAS — I

I. Introduction

Recent advances in the technology for producing gas puff plasmas has made them very attractive as high brightness laboratory x-ray radiation sources. In addition, it has become evident that the gas puff technology can be employed to investigate a number of interesting x-ray laser schemes. In fact, Sandia National Laboratory has carried out a program involving the implosion of a gas puff plasma onto a low density foam to determine the feasibility of creating a homogeneous, uniform gain medium along the central core axis.[1] The preliminary experimental results indicate high radiative conversion efficiencies from relatively clean, reproducible implosions.

In this investigation, which is the first in a series of reports, we seek to determine a better understanding of imploding gas puff plasmas for a varity of conditions and configurations, particularly the radiation hydrodynamics with and without a central core plasma. We will also explore the consequences of invoking a number of approximations and their impact on the results. For instance, are radiative losses of sufficient magnitude to warrant a self-consistent radiation hydrodynamics treatment? How does opacity affect the overall implosion dynamics? Does the transport of energy in the plasma modify the implosion hydrodynamics? What detail is required to accurately model the radiation? How does LTE or corona equilibrium compare with CRE? We hope to shed some light on these and other issues relevant to an accurate description and understanding of imploding gas puff plasmas.

Manuscript approved May 8, 1985.

II. Theoretical Model

Since the implosion of a cylindrical gas puff plasma can result in a substantial fraction of the total plasma energy being radiated away, the pure hydrodynamic evolution of the plasma may be modified. Thus, because of the nonlinear nonlocal interactions, the hydrodynamic development, atomic and radiation physics of the plasma, as well as the transport of radiation, must be calculated self-consistently.

Discussion of the theoretical model can be separated for convenience as follows: (a) hydrodynamics and thermal conduction (b) ionization and atomic physics and (c) radiation emission and transport.

(A) Hydrodynamics and Thermal Conduction

The basic hydrodynamic variables of mass, momentum, and total energy are transported in one dimension using a numerical scheme with a sliding-zone version of flux-corrected transport.[2] A special gridding algorithm is used which moves zones in a Lagrangian fashion and adjusts the mesh in order to resolve steep gradients in the flow. The hydrodynamic equations solved are

$$\frac{D\rho}{Dt} = \frac{\partial\rho}{\partial t} + \nabla \cdot (u\rho) = 0 \qquad (1)$$

$$\frac{D(\rho u)}{Dt} = -\nabla P \qquad (2)$$

$$\frac{D\varepsilon_T}{Dt} = -\nabla \cdot (uP) + \dot{\varepsilon}_{rad} + \nabla \cdot (\eta N \nabla T) \qquad (3)$$

where ρ is mass density, u is velocity, P is pressure, ε_T is total energy density, $\dot{\varepsilon}_{rad}$ is the rate of energy loss or gain due to radiation, η is the thermal conductivity, and N is the ion density. The thermal conduction is calculated implicitly, using an iterative Crank-Nicholson scheme.

Since the density generally did not exceed solid density in this study, a simple equation of state was assumed, viz.

$$P = \frac{2}{3} (\varepsilon_T - \frac{1}{2} \rho u^2 - \varepsilon_I) , \qquad (4)$$

where ε_I is the potential energy due to ionization and excitation. (A non-ideal equation of state taking account of ionization energy and degeneracy pressure can be employed in cases where the density exceeds solid density.) A single temperature model was employed,

$$kT = \frac{P}{(\rho/m_I)\ (1+\bar{Z})} , \qquad (5)$$

where m_I is ion mass, and T is temperature. The ionization energy, ε_I, and effective charge, Z are calculated from the ionization-radiation equations which are explained below. A single temperature assumption is valid in the core plasma, where the equilibration time is of the order of picoseconds, and it is adequate in the stagnation region, where the equilibration time can be of the order of nanoseconds. In the blowoff plasma, it is a marginal approximation, but the consequences are minor, since little radiation is emitted from this region, and most of the thermal energy is carried by the electrons in the blowoff.

The local rate of change of energy due to radiation transport, $\dot{\varepsilon}_{rad}$, will be discussed below.

(B) Ionization and Atomic Physics

The ionic populations in the plasma are determined by a set of atomic rate equations of the form

$$\frac{df_i}{dt} = \sum_j W_{ji} f_j - \sum_i W_{ij} f_i \tag{6}$$

where f_i is the fractional population of atomic level i, and W_{ji} is the net reaction rate describing the transition from initial state j to final state i. An equation of this type is constructed for each of the atomic levels included in the model.

For sufficiently dense plasmas, the effective populating and depopulating rates are generally fast compared with the hydrodynamic response. Under these circumstances, an equilibrium assumption can be justified, which involves dropping the explicit time dependence in Eq. (6). The plasma is then said to be in collisional-radiative equilibrium (CRE),[3] whereby the plasma ionization state responds instantaneously to changes in hydrodynamic quantities.

The rate coefficients that are used to calculate the populating and depopulating rates, W_{ji}, are calculated using various atomic calculational methods. The processes included in this calculation and the methods used in calculating the corresponding rate coefficients are summarized elsewhere.[4-10]

Once the set of rate equations (including the optical pumping from the radiation field) has been solved for the level populations f_i, the electron density can be calculated,

$$N_e = \sum_i z_i \; f_i \; N_I \tag{7}$$

where z_i is the ionic charge of level i and N_I is the total ion density.

The ionization and excitation energy can also be calculated by

$$\varepsilon_i = \sum_i \chi_i \; f_i \; N_I \; , \tag{8}$$

where χ_i is the energy of level i, measured from the ground state of the neutral atom.

For the simulations presented below, the atomic model for neon contains 27 atomic levels and 13 emission lines.

(C) Radiation Emission and Transport

Radiation emission from and absorption by a plasma are dependent on the local atomic level population densities. Except for optically thin plasmas, however, the level populations depend on the radiation field, since optical pumping via photoionization and photoexcitation can produce significant population redistribution. Thus, the ionization and radiation transport processes are strongly coupled and must be solved self-consistently. In this model, an iterative procedure[11] is used, where level populations are calculated using the radiation field from the previous iteration, then using these populations to calculate a new radiation field and recalculating populations until convergence is reached.

A probabilistic radiation transport scheme[12,13] was employed, which forms local angle and frequency averaged escape probabilities for each emission line and for each bound-free process. Free-free radiation is treated with a multifrequency transport formalism. The radiation transport and emission spectra are calculated from these escape probabilities. The method can treat comprehensive atomic models and provides good overall energetics, but cannot calculate accurately certain spectral details and lines with very high optical depths.

Inner-shell opacities are included in the model, since these processes are very important in the cool, dense plasma regions. Inner-shell photoionization cross sections for the neutral element are taken from the fits by Biggs and Lighthill,[14] and the positions of the ionization-dependent absorption edges are taken from the Hartree-Fock calculations of Clementi and Roetti.[15]

The local rate of energy change in zone j, due to radiation transport is given by

$$\dot{\varepsilon}_j = - \sum_P (F_{Pj} - \sum_k C_{Pkj} F_{Pk}) \qquad (9)$$

where F_{Pk} is the rate of energy loss in zone k due to a discrete radiative process (or frequency group) P, and C_{Pkj} is the radiative coupling of zone k to zone j for that process. The couplings are functions of opacity, integated over process and photon path. In the probabilistic model, a matrix of couplings must be computed for each bound-bound, bound-free and free-free process. In this way, the net cooling and heating by radiation emission and absorption between the various zones of the plasma is accurately taken into account.

III. Results

(A) Puff-Gas Implosion with a Central Core Plasma

Simulations were performed for a cylindrical annular neon puff-gas of density 5×10^{-6} g/cm^3, with inner radius 0.55 cm and outer radius 1.95 cm, imploding radially at a velocity of 3×10^{7} cm/sec. Results were obtained with and without a central neon core plasma of density 5×10^{-3} g/cm^3 and radius 0.10 cm. The initial configuration with the core plasma is shown in Fig. 1. The temperature of the puff-gas was taken to be about 5 eV initially, and the core plasma temperature was about 0.04 eV. A tenuous background plasma was placed between the puff-gas and core plasmas of density 5×10^{-7} g/cm^3. These initial conditions were chosen to correspond approximately to experiments being conducted at Sandia National Laboratory.[1]

Results of simulations with a central core plasma will be discussed first. For the first 15 nanoseconds, the puff-gas plasma essentially coasts radially inward. The forward edge of the puff gas is heated to a few tens of eV through accretion of background plasma. At about 15 nanoseconds, the puff-gas makes full contact with the core, and conversion of kinetic energy to thermal energy at the interface creates a large overpressure. The plasma temperature quickly exceeds 100 eV in the contact region, and a narrow region of intense net radiative emission centered at the interface is formed.

At 40 nanoseconds (Fig. 2), the peak temperature near the interface exceeds 300 eV, and the overpressure has

caused shocks to propagate radially inward in the core plasma and outward in the puff gas. Heating from the soft x-rays produced in the interface region is evident in the dense core, and radiation heating is also taking place deep in the puff gas. The effects of radiation transport will be more clearly seen when comparison is made with a radiationless simulation. Thermal conduction creates a nearly isothermal region near the leading edge of the puff gas, but it is ineffective in transporting energy into the core.

By 50 nanoseconds (Fig. 3), the inward propagating shock has reached the origin. Although the plasma approaches solid density on axis, the temperature there is still only a few tens of eV. This region of very dense plasma is radiating strongly in the L-shell, but its volume is small. A broader annulus of hot plasma, situated outside the core plasma is producing most of the K- and L-shell radiation. The emission spectrum at 50 nanoseconds is shown in Fig. 4. The spectral power is about evenly divided between continuum and line radiation at this time; almost half of the total power is carried by the K-shell emission lines Ne X 2p-1s and Ne IX 2p-1s.

At 70 nanoseconds (Fig. 5) the entire plasma is moving radially outwards. The core plasma remains cool, since the density is still high enough to retard thermal conduction. Furthermore, the radiative emission of this region is in approximate balance with the radiative absorption.

The energy history of the plasma throughout the first 120 nanoseconds is shown in Fig. 6. Initially, about 98% of the total energy is kinetic; the remainder is in thermal and

ionization energies. The energy lost to radiation begins to increase sharply just before 20 nanoseconds, as the puff gas comes into contact with the central core. Thermal and ionization energies also begin to increase sharply at this time. Kinetic energy goes through a well defined minimum at about 60 nanoseconds, at which time almost half of the total plasma energy has been radiated away. Although peak compression on axis occurs at about 50 nanoseconds, substantial portions of the puff gas plasma continue to move radially inward until about 60 nanoseconds. By 120 nanoseconds about two-thirds of the total energy has been converted to radiation.

A similar calculation was performed without radiation effects, but with detailed atomic physics, so that the ionization and excitation energies and electron number densities would be self-consistently calculated. Although radiative cooling and optical pumping were turned off, optically thin radiation was calculated for comparison with the simulation discussed above.

At 40 nanoseconds (Fig. 7), the profiles are qualitatively very similar to those with radiation effects. However, the role of radiation in transporting energy is clearly evident. The dense core is still very cold compared with the complete simulation with radiation transport. Also, the temperatures in the puff-gas plasma differ by a factor of about three. The heating of the puff-gas out to about 0.8 cm evident in Fig. 2 is the direct result of radiation transport. Temperature and density gradients in the inward propagating shock are steeper in the radiationless case; however, assembly occurs at about the same time.

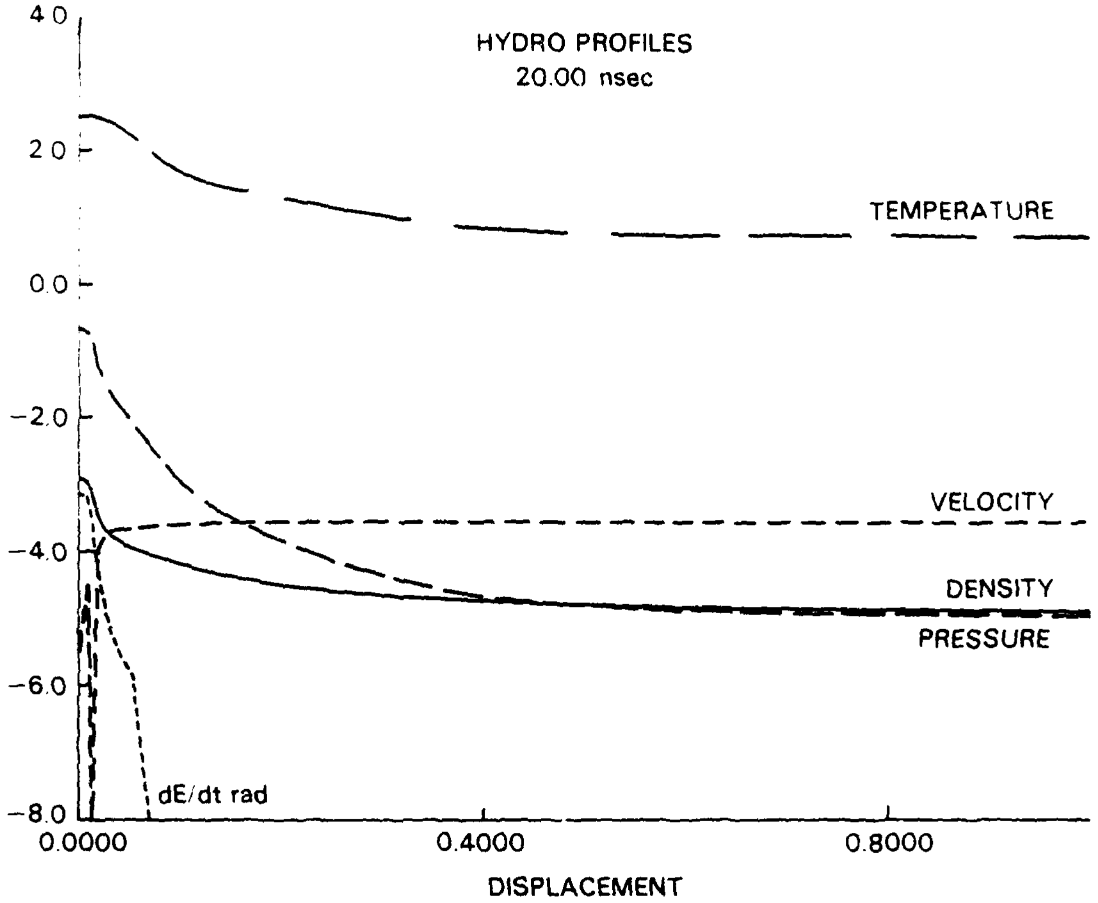

Fig. 9. Profiles at 20 nanoseconds for radiation-hydrodynamics calculation without a central core. Temperature and density at the origin are near peak values; as plasma continues to flow inward, the volume of hot moderately dense plasma will increase.

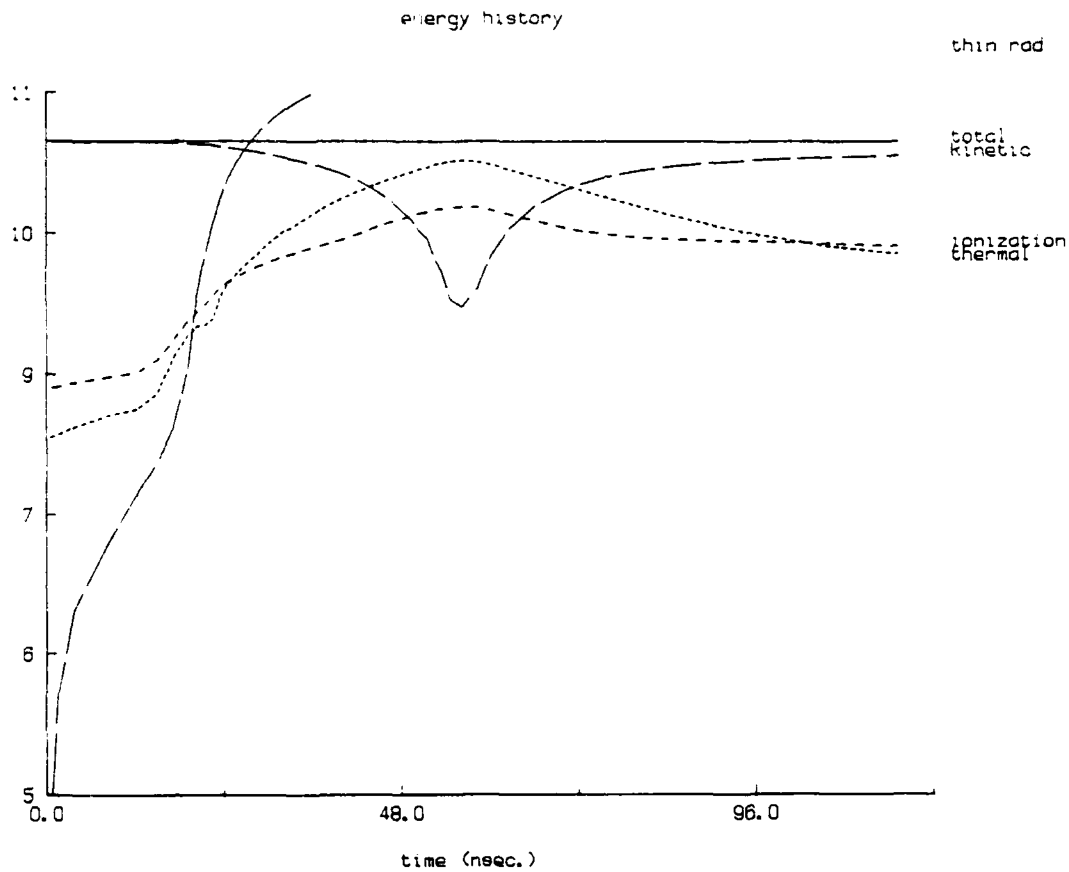

Fig. 8. Energy partition for puff gas implosion with a central core, but neglecting the effects of radiation. Now the total energy is synonymous with the plasma energy. Optically thin radiation is plotted for purposes of comparison, but it does not remove energy from the plasma. The relative minimun in kinetic energy occurs somewhat earlier, and the energies are substantially different from those in Fig. 6 after 30 nanoseconds.

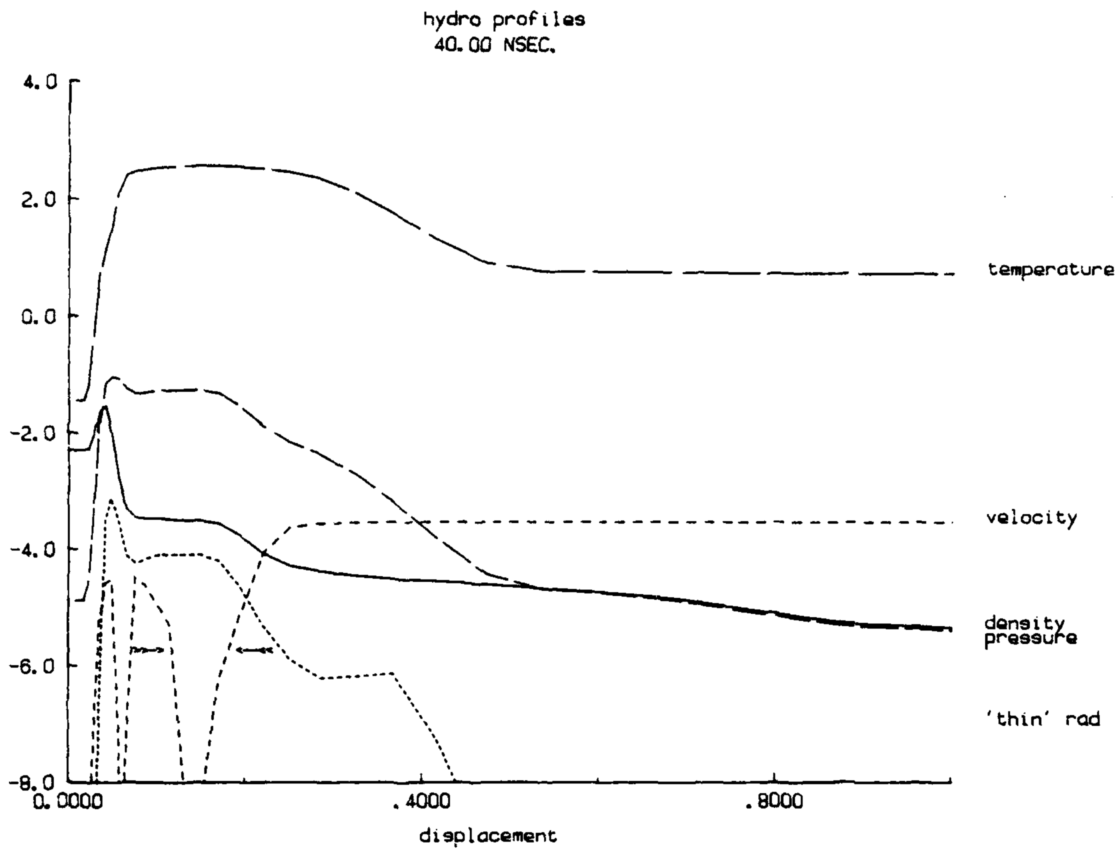

Fig. 7. Profiles at 40 nanoseconds with a central core neglecting the effects of radiation. The core plasma remains very cold and there is no evidence of heating deep in the puff-gas.

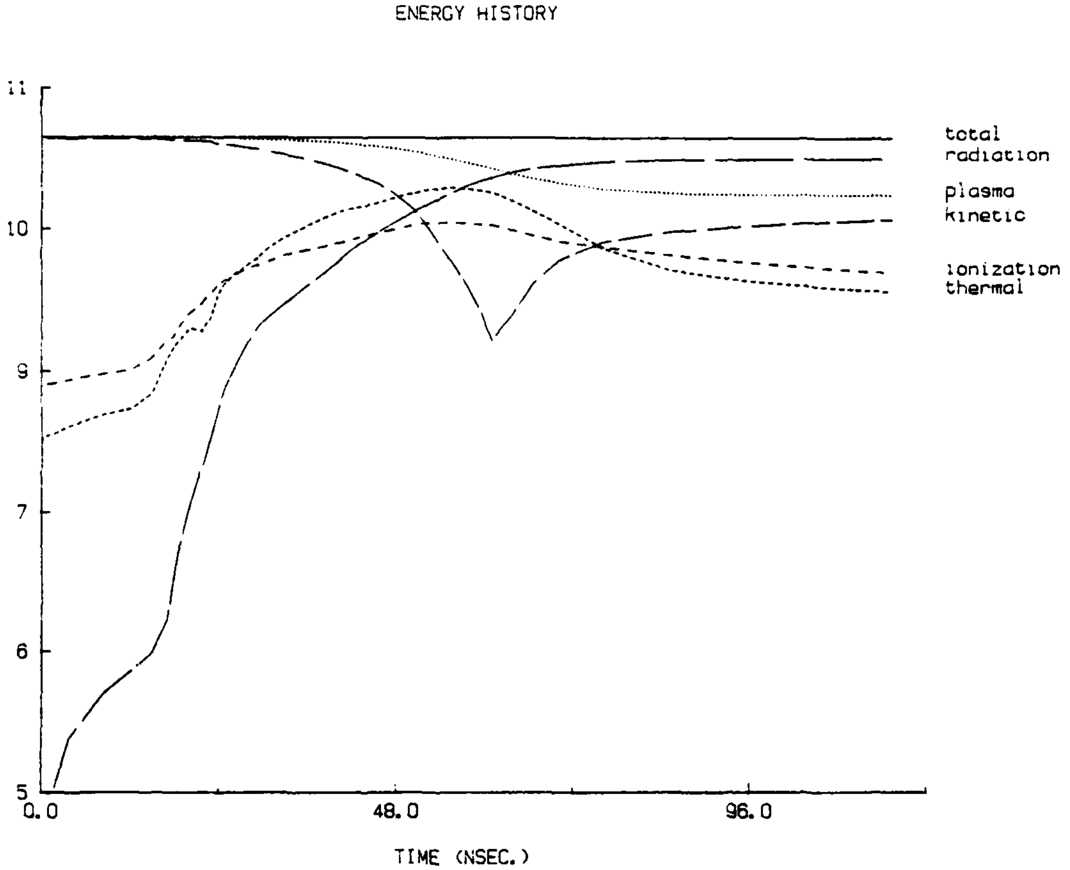

Fig. 6. Energy partition for puff gas implosion with a central core. Total energy, which remains constant in time, is the sum of the energy lost to radiation and the energy which remains in the plasma. The plasma energy is the sum of the kinetic, ionization and thermal energies. The energies ($\log_{10}$ energy in ergs) are given as a function of time (in nanoseconds).

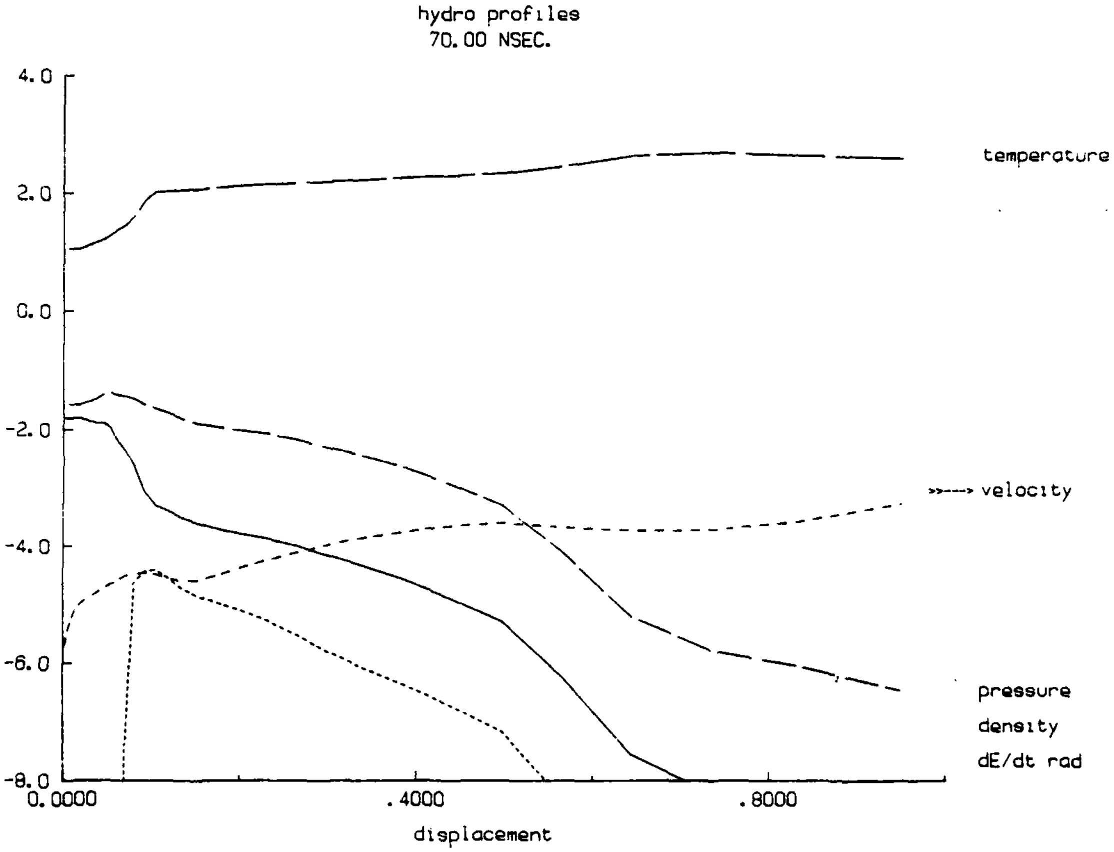

Fig. 5. Profiles at 70 nanoseconds for radiation-hydrodynamic calculation with a central core. Expansion phase: the entire plasma is now moving radially outwards. The core plasma remains cool.

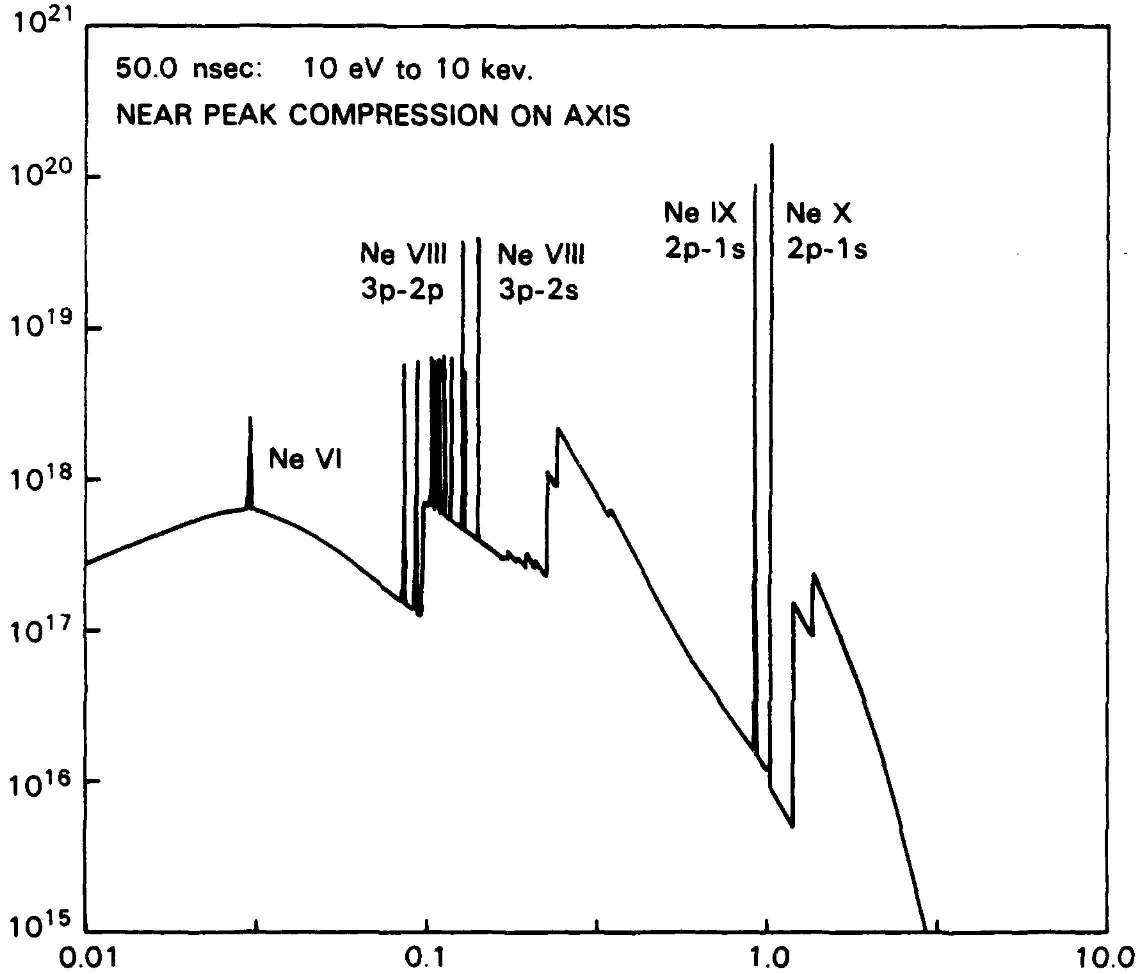

Fig. 4. Emission spectrum at 50 nanoseconds. Spectral intensity (from 10^{15} to 10^{21} ergs/sec-cm-keV) is plotted as a function of photon energy (from 10 eV to 10 keV). K-shell radiation dominates at this time with most of the power in the indicated H and He-like emission lines.

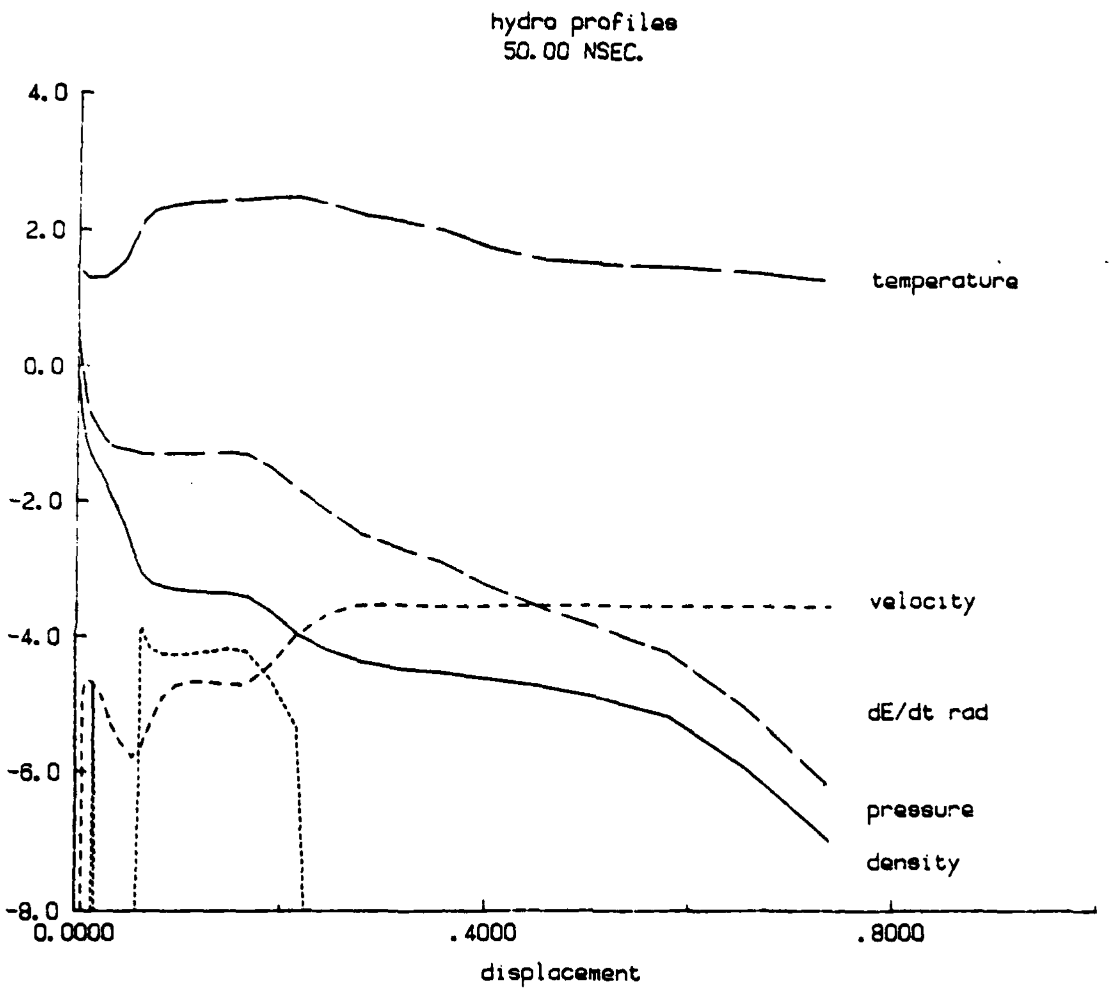

Fig. 3. Profiles at 50 nanoseconds for radiation-hydrodynamics calculation with a central core. Assembly phase: inward propagating shock reaches axis; peak density approaches solid density. Bulk of plasma is still moving radially inwards.

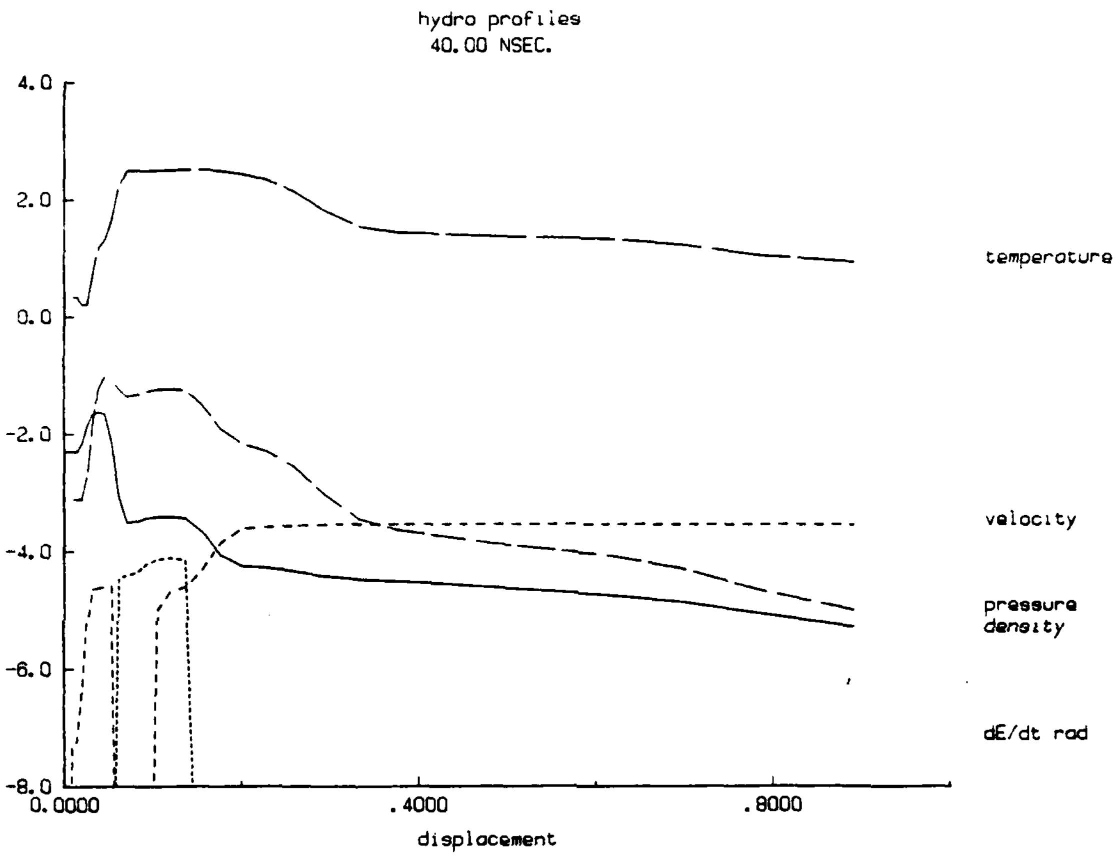

Fig. 2. Profiles at 40 nanoseconds for radiation-hydrodynamics calculation with a central core. Inward and outward propagating shocks have been formed. Radiation transport has heated core plasma and puff gas out to about 0.8 cm. Radial displacement is given in cm., $\log_{10}$ density in g/cm^3, $\log_{10}$ temperature in eV, $\log_{10}$ pressure in ergs/cm^3 x 10^{-12}, $\log_{10}$ velocity in cm/nsec x 10^{-2} and $\log_{10}$ $\dot{\varepsilon}_{rad}$ in ergs/cm^3-nsec x 10^{-14}.

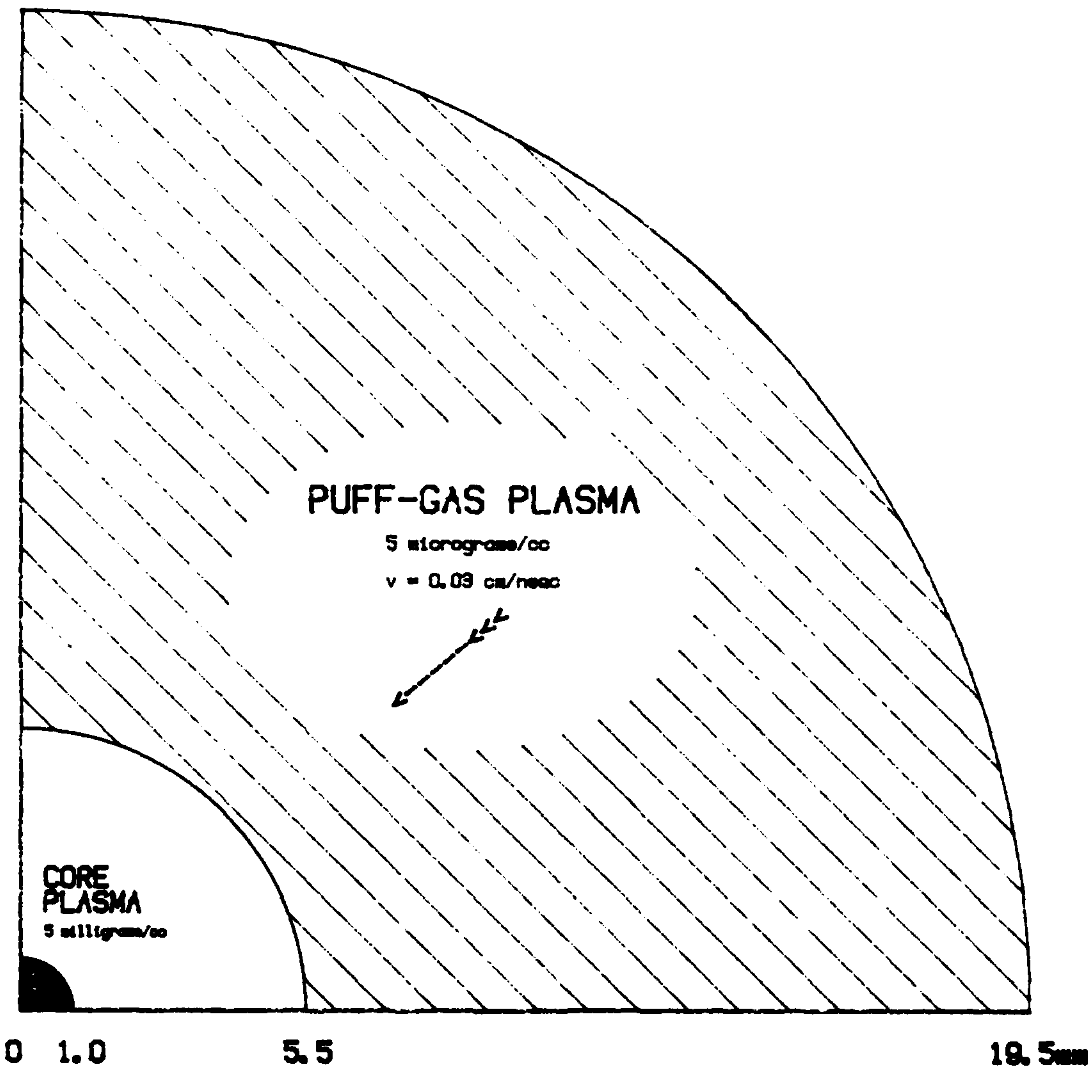

Fig. 1. Initial Configuration: Puff gas plasma is imploding at 0.03 cm/nsec onto a low density core.

ACKNOWLEGMENTS

The authors would like to thank Dr. D. Duston, and Dr. F. Cochran for their interest and assistance in this investigation. We would like to particularly thank Dr. J. Farber for his suggestion of investigating the double gas puff some years ago and for his continued interest in this work. This work was supported by the Defense Nuclear Agency.

hydrodynamic response, a self-consistent calculation, linking radiation and fluid transport with the ionization dynamics, must be performed. The "hydrodynamic" calculation, which was compared to the self-consistent simulation, neglected radiation but included ionization dynamics. At certain times and regions, the local energy of ionization and excitation substantially exceeded the local thermal energies. A pure "hydrodynamic" calculation with simplified prescriptions for ionization energy and average ionization state would produce a substantially different plasma evolution, leading to erroneous conclusions.

Since radiation plays such a crucial role, it must be generated and transported accurately. As we have shown, optically thin radiation ignores the importance of transport of radiative energy and grossly overestimates losses. LTE or corona equilibrium models for the level populations will also lead to inaccurate energetics. We found that the atomic populations in the regions of peak radiative emission were substantially different from corresponding LTE or corona equilibrium populations, in some cases by orders of magnitude.

Accurate radiation energetics demands a sufficiently detailed atomic model. The simple neon model employed here underestimates the radiation losses by about a factor of two. Thus, we plan to perform similar calculations with a full neon model to assess and determine its influence on the plasma evolution, radiative yields, and spectrum.

radiation losses under these circumstances. Ultimately, the optically thin treatment overestimates energy loss by almost a factor of two.

The simulations described above were carried out with a relatively simple atomic model for neon. How much accuracy has been given up by using a reduced model? The hydrodynamic profiles of Fig. 9 were post-processed using a full neon K- and L-shell model, and the resulting spectrum is shown in Fig. 14. Not only are there more emission lines, but the radiative power in some of the most important lines is substantially increased, as is the continuum radiation. The ionization state of the plasma is actually increased, reflecting the increased probability of ionization from the excited levels (which are included). The total radiated power is slightly more than a factor of two larger than that calculated with the simple model.

IV. Conclusions

Puff-gas implosions show promise as a means of efficiently converting kinetic energy to radiation. Higher plasma densities and total radiative yields can be achieved through the use of a central core plasma. In the case we studied using a core, more than two-thirds of the total plasma energy was converted to K- and L-shell radiation. Without a core plasma, total radiative yield is smaller, but the fraction of K-shell radiation is larger, due to the reduced plasma mass.

Because the radiative energy loss and the transport of radiation in the plasma substantially modify the

emission spectrum at 20 nanoseconds is given in Fig. 10. More than 75% of the spectral power is carried by the K-shell lines. Plasma continues to flow inward and stagnate, and, although the peak density falls somewhat, by 40 nanoseconds, a substantially larger volume of plasma is radiating. Since the temperature remains about the same, the emission spectrum at 40 nanoseconds is qualitatively very similar, but shifted upward in intensity by about an order of magnitude (Fig. 11).

The energy history of the implosion is given in Fig. 12. It is similar to that with a central core plasma (Fig. 6), especially during the first 50 nanoseconds. In the present case, the radiated energy rises even more rapidly, and actually exceeds the yield with a central core until about 50 nanoseconds. Ultimately, slightly more than half of the total plasma energy is radiated away. The plasma kinetic energy exhibits a more pronounced minimum at a slightly later time. Thus, the fraction of the total energy radiated away is significantly larger with a central plasma core, but the additional mass results in a smaller average temperature, and the fraction of K-shell radiation is substantially smaller.

A simulation was performed for the case without a core neglecting radiation effects. The energy history for this calculation is shown in Fig. 13. Because of the absence of radiative cooling, thermal energies are higher, and the kinetic energy minimum occurs sooner. Optically thin radiation, which was calculated but not used to cool the plasma, is observed to rise rapidly, even before ten nanoseconds. Opacity effects would substantially reduce

A corresponding energy history of this simulation is shown in Fig. 8. The early history is similar to that shown in Fig. 6. By 30 nanoseconds, however, substantially more energy resides in thermal and ionization energies. The relative minimum in kinetic energy occurs earlier and is not as sharp. The difference in timing can be attributed to the role of radiation in reducing the overpressure in the interface region. As can be seen from the optically thin radiation curve, radiative cooling can be greatly overestimated in problems of this type if opacity effects are not included.

(B) Puff-Gas Implosion Without a Core Plasma

A series of simulations without a core plasma were performed, assuming the same puff gas density of $5X10^{-6}$ g/cm^3 and temperature of 5 eV. As before, the inner and outer radii of the puff gas were taken to be 0.55 cm and 1.95 cm, respectively, with a radial velocity of $3X10^7$ cm/sec. A background plasma of density $5X10^{-7}$ g/cm^3 filled the central void.

During the coasting phase, lasting about 18 nanoseconds, the puff gas moves radially inward, accreting background plasma and warming to a few tens of eV at its forward edge. Rapid heating and compression take place as the puff gas reaches the origin. Figure 9 shows the situation at 20 nanoseconds. Peak density is about 1.3×10^{-3} g/cm^3 and temperature near the axis is slightly above 300 eV. The hot, moderately dense plasma near the origin is radiating strongly in the K-shell, but its volume is small. The

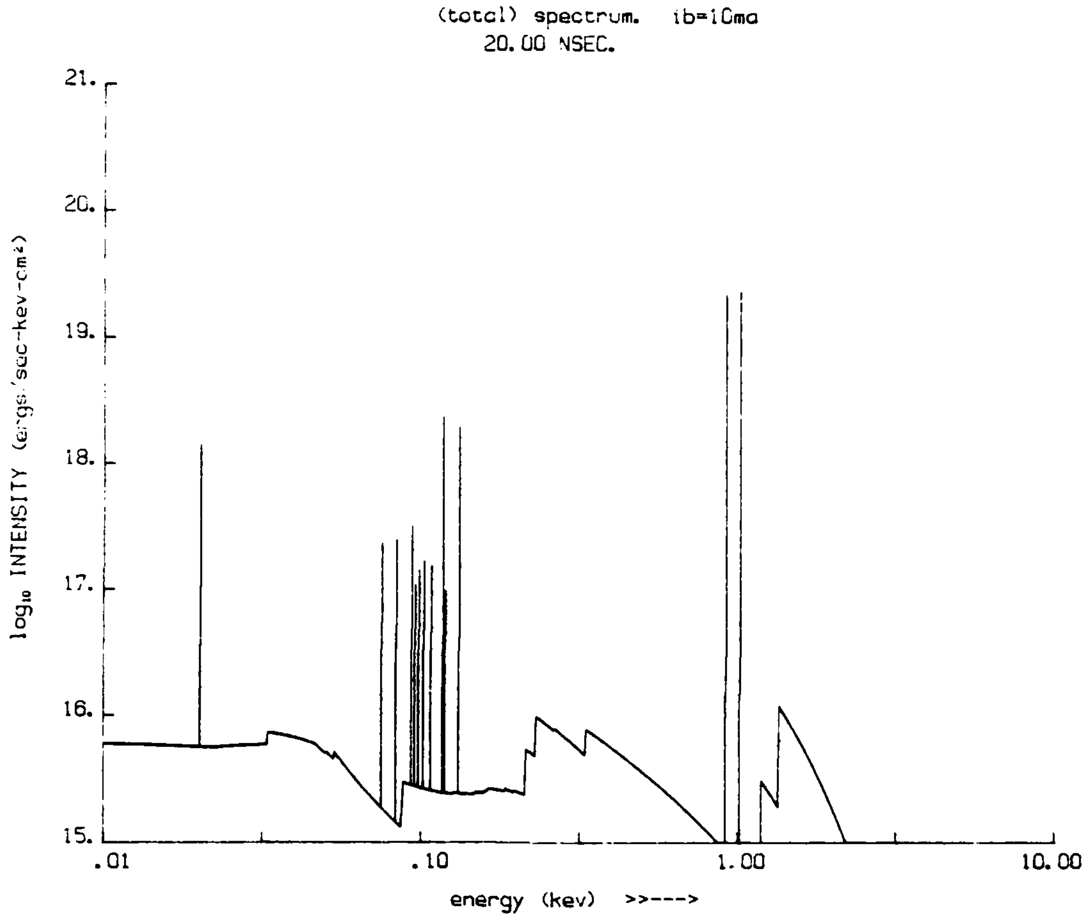

Fig. 10. Emission spectrum at 20 nanoseconds. Without a core, the spectrum is "hotter", with proportionately more k-shell radiation, than with a central core.

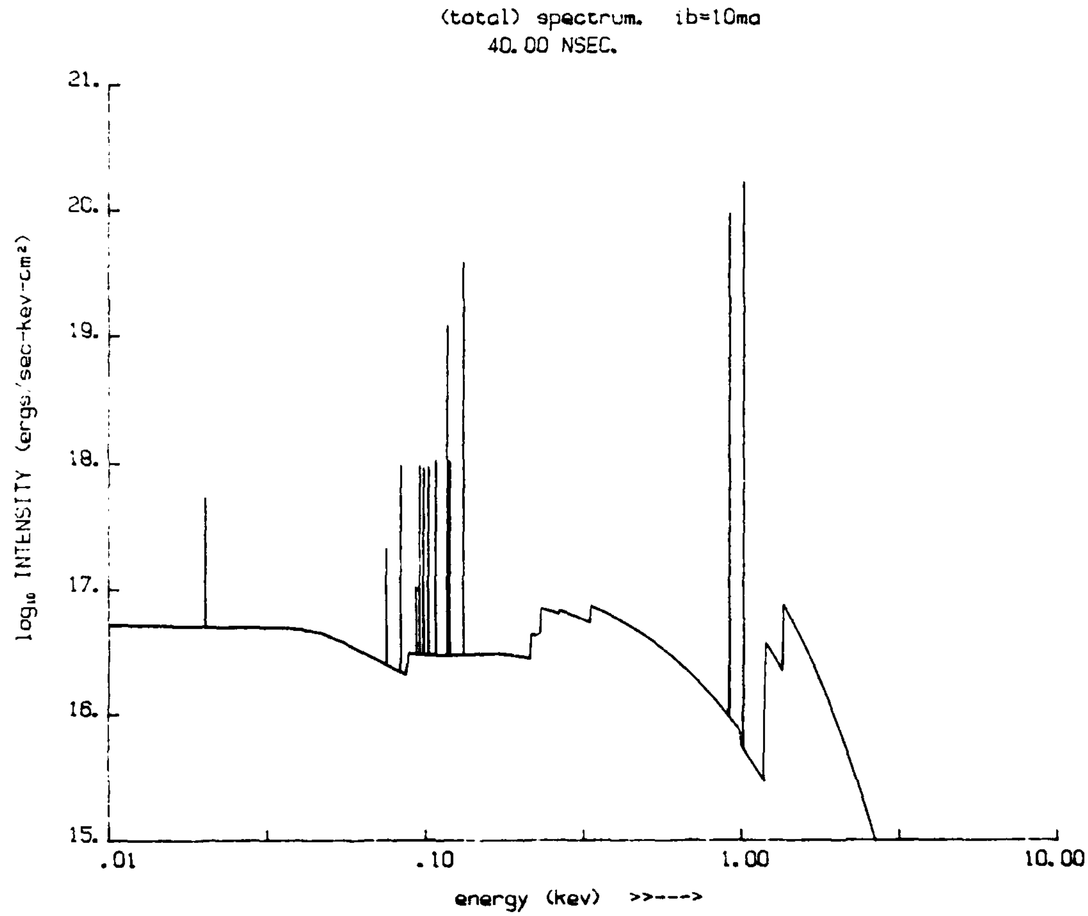

Fig.11. Emission spectrum at 40 nanoseconds. As the volume of radiating plasma increases, the radiated power increases; however, the temperature changes only slightly. The resulting spectrum closely resembles that of Fig. 10 shifted upward in intensity.

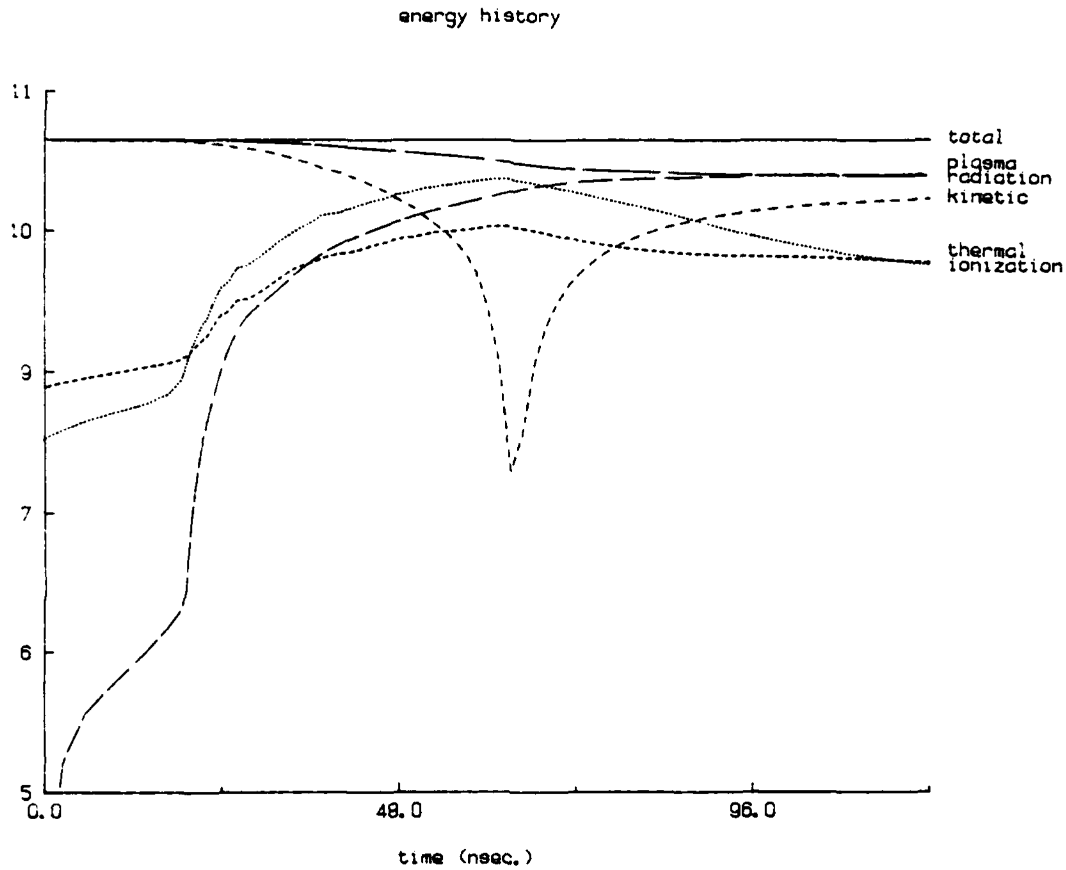

Fig. 12. Energy partition for puff gas implosion without a central core. Although radiation energy increases more rapidly at early times without a core, only about half of the total energy is radiated away by 100 nanoseconds, compared with about two-thirds in the case with a core.

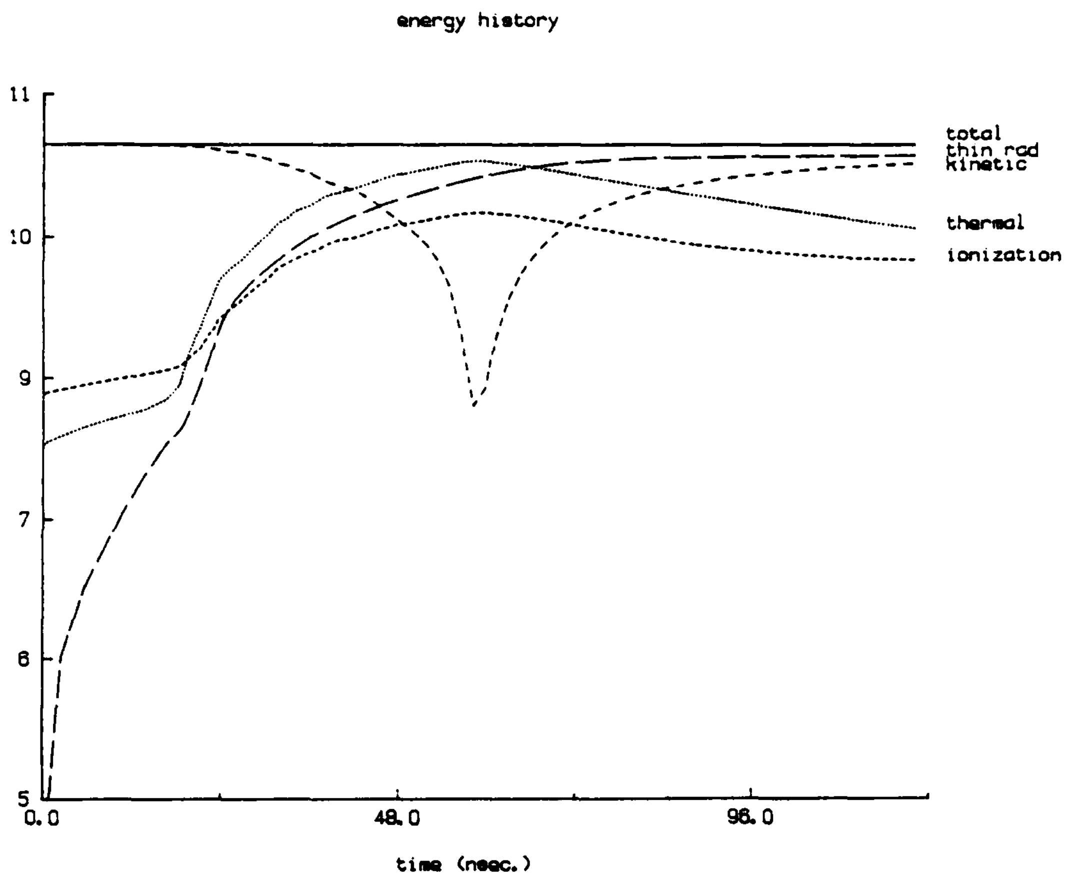

Fig. 13. Energy partition for puff-gas implosion neglecting the effects of radiation. Optically thin radiation is plotted for purposes of comparison, but it does not remove energy from the plasma.

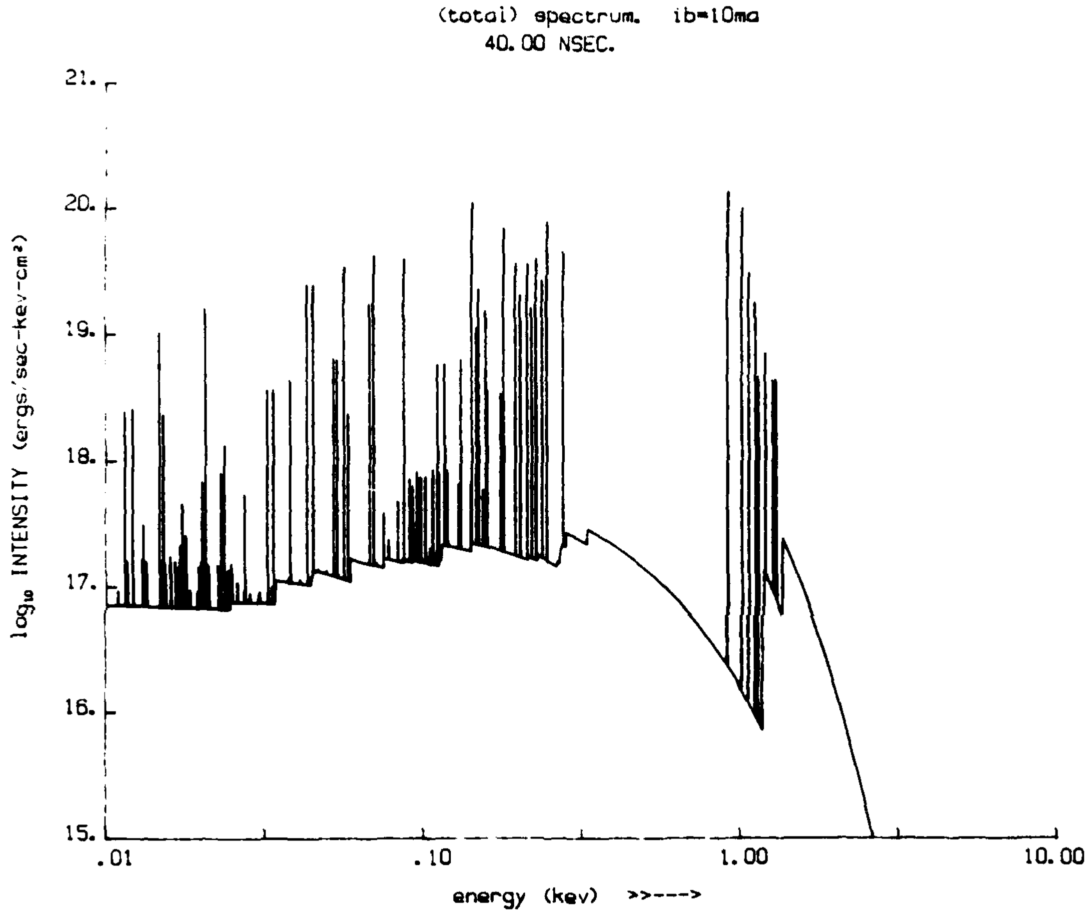

Fig. 14. Emission spectrum at 40 nanoseconds with complete atomic model for neon. Comparison should be made with Fig. 11. Substantially increased radiative power in both emission lines and continuum. Ionization of plasma is increased due to inclusion of more excited levels.

References

1. R. Spielman and M.A. Palmer, Bull. Amer. Phys. Soc., 24,1361 (1984).

2. J. P. Boris and D. L. Book, J. Comput. Phys. 11,38 (1973).

3. D. Duston and J. Davis, Phys. Rev. A 23,2602 (1981).

4. D. R. Bates, A. E. Kingston, and R. W. P. McWhirter, Proc. R. Soc. London, Ser. A 267,297 (1962).

5. A. Burgess, in Proceedings of the Symposium on Atomic Collision Proceedings of the Symposium on Atomic Collision Processes in Plasmas, Culham, England, Report No. 4818, 63, 1964 (unpublished); and A. Burgess, H. P. Summers, D. M. Cochrane, and R. W. P. McWhirter, Mon. Not. R. Astron. Soc. 179,275 (1977).

6. V. L. Jacobs, J. Davis, P. C. Kepple, and M. Blaha, Astrophys. J. 211,605 (1977).

7. W. J. Karzas and R. Latter, Astrophys. J. Suppl. Ser. 6,167 (1961).

8. V. L. Jacobs and J. Davis, Phys. Rev. A 18,697 (1978).

9. J. Davis, P. C. Kepple, and M. Blaha, J. Quant. Spectrosc. Rad. Transfer 16,1043 (1977).

10. E. Oran and J. Davis, J. Appl. Phys. 45,2480 (1974).

11. J. P. Apruzese, J. Davis, D. Duston and R. W. Clark, Phys. Rev. A 29,246 (1984).

12. J. P. Apruzese, J. Davis, D. Duston, and K. G. Whitney, J. Quant. Spectrosc. Rad. Transfer 23,479 (1980).

13. J. P. Apruzese, P. C. Kepple, K. G. Whitney, J. Davis and D. Duston, Phys. Rev. A 24,1001 (1981).

14. Frank Biggs and Ruth Lighthill, Sandia Laboratories Report No. SC-RR-71 0507, 1971 (unpublished).

15. E. Clementi and C. Roetti, At. Data Nucl. Data Tables 14,177 (1974).

DISTRIBUTION LIST

Assistant to the Secretary of Defense Atomic Energy Washington, D.C. 20301 ATTN: Executive Assistant	1 Copy
Defense Technical Information Center Cameron Station 5010 Duke Street Alexandria, Va 22314	2 copies
Director Defense Intelligence Agency Washington, D.C. 20301 ATTN: DT-1B R. Rubenstein	1 Copy
Director Defense Nuclear Agency Washington, D.C. 20305	
ATTN: DDST	1 copy
ATTN: TITL	4 copies
ATTN: RAEV	1 copy
ATTN: STVI	1 copy
Commander Field Command Defense Nuclear Agency Kirtland AFB, New Mexico 87115 ATTN: FCPR	1 Copy
Chief Field Command Livermore Division Department of Defense P.O. Box 808 Livermore, CA 94550 ATTN: FCPRL	1 Copy
Director Joint Strat TGT Planning Staff Offutt AFB Omaha, Nebraska 68113 ATTN: JSAS	1 Copy

Undersecretary of Defense
  for RSCH and ENGRG
Department of Defense
Washington, D.C. 20301
    ATTN: Strategic and Space Systems (OS)
	1 Copy

Deputy Chief of Staff for RSCH DEV and ACQ | 1 Copy
Department of the Army
Washington, D.C. 20301
ATTN: DAMA-CSS-N

Commander | 1 copy each
Harry Diamond Laboratories
Department of the Army
2800 Powder Mill Road
Adelphi, MD 20783
ATTN: DELHD-N-NP
ATTN: DELHD-R J. Rosado
ATTN: DELHD-TA-L (Tech. Lib.)

U.S. Army Missile Command
Redstone Scientific Information Center | 3 Copies
Attn: DRSMI-RPRD (Documents)
Redstone Arsenal, Alabama 35809

Commander | 1 copy
U.S. Army Missile Command
Redstone Arsenal, Alabama 35898
ATTN: DRCPM-PE-EA

Commander
U.S. Army Nuclear and Chemical Agency
7500 Backlick Road | 1 copy
Building 2073
Springfield, VA 22150
ATTN: Library

Commander | 1 Copy
Naval Intelligence Support Center
4301 Suitland Road, Bldg. 5
Washington, D.C. 20390
ATTN: NISC-45

Commander | 1 Copy
Naval Weapons Center
China Lake, California 93555
ATTN: Code 233 (Tech. Lib.)

Officer in Charge | 1 Copy each
White Oak Laboratory
Naval Surface Weapons Center
Silver Spring, Md. 20910
ATTN: Code R40
ATTN: Code F31

Air Force Weapons Laboratory Kirtland AFB, New Mexico 87117 ATTN: SUL ATTN: CA ATTN: APL ATTN: Lt. Col Generosa	1 Copy each
Deputy Chief of Staff Research, Development and Accounting Department of the Air Force Washington, D. C. 20330 ATTN: AFRDQSM	1 Copy
Commander U.S. Army Test and Evaluation Command Aberdeen Proving Ground, MD 21005 ATTN: DRSTE-EL	1 Copy
Space and Missile Systems Organization/SK Air Force Systems Command Post Office Box 92960 Worldway Postal Center Los Angeles, CA 90009 ATTN: SKF P. Stadler (Space Comm. Systems)	1 Copy
AVCO Research and Systems Group 201 Lowell Street Wilminton, MA 01887 ATTN: Library A830	1 Copy
BDM Corporation 7915 Jones Branch Drive McLean, Virginia 22101 ATTN: Corporate Library	1 Copy
Berkeley Research Associates P.O. Box 983 Berkeley, CA 94701 ATTN: Dr. Joseph Workman	1 Copy
Berkeley Research Associates P.O. Box 852 5532 Hempstead Way Springfield, VA 22151 ATTN: Dr. Joseph Orens ATTN: Dr. Nino Pereira	1 Copy each
Boeing Company P. O. Box 3707 Seattle, WA 98134 ATTN: Aerospace Library	1 Copy

The Dikewood Corporation 1613 University Bldv., N.E. Albuquerque, New Mexico 8710 ATTN: L. Wayne Davis	1 Copy
EG and G Washington Analytical Services Center, Inc. P. O. Box 10218 Albuquerque, New Mexico 87114 ATTN: Library	1 Copy
General Electric Company Space Division Valley Forge Space Center P. O. Box 8555 Philadelphia, PA 19101 ATTN: J. Peden	1 Copy
General Electric Company - Tempo Center for Advanced Studies 816 State Street P.O. Drawer QQ Santa Barbara, CA 93102 ATTN: DASIAC	1 Copy
Institute for Defense Analyses 1801 N. Beauregard St. Alexandria, VA 22311 ATTN: Classified Library	1 Copy
IRT Corporation P.O. Box 81087 San Diego, CA 92138 ATTN: R. Mertz	1 Copy
JAYCOR 11011 Forreyane Rd. P.O. Box 85154 San Diego, CA 92138 ATTN: E. Wenaas	1 Copy
JAYCOR 205 S. Whiting Street, Suite 500 Alexandria, VA 22304 ATTN: R. Sullivan	1 Copy
KAMAN Sciences Corp. P. O. Box 7463 Colorado Springs, CO 80933 ATTN: J. Hoffman ATTN: A. Bridges ATTN: D. Bryce ATTN: W. Ware	1 copy each

Lawrence Livermore National Laboratory University of California P.O. Box 808 Livermore, California 94550 Attn: DOC CDN for L-153 Attn: DOC CDN for L-47 L. Wouters Attn: DOC CDN for Tech. Infor. Dept. Lib.	1 copy each
Lockheed Missiles and Space Co., Inc. P. O. Box 504 Sunnyvale, CA 94086 Attn: S. Taimlty Attn: J.D. Weisner	1 copy each
Lockheed Missiles and Space Co., Inc. 3251 Hanover Street Palo Alto, CA 94304 Attn: J. Perez	1 Copy
Maxwell Laboratory, Inc. 9244 Balboa Avenue San Diego, CA 92123 ATTN: A. Kolb ATTN: M. Montgomery ATTN: J. Shannon	1 Copy each
McDonnell Douglas Corp. 5301 Bolsa Avenue Huntington Beach, CA 92647 ATTN: S. Schneider	1 Copy
Mission Research Corp. P. O. Drawer 719 Santa Barbara, CA 93102 ATTN: C. Longmire ATTN: W. Hart	1 Copy each
Mission Research Corp.-San Diego 5434 Ruffin Rd. San Diego, California 92123 ATTN: Victor J. Van Lint	1 Copy
Northrop Corporation Northrop Research and Technology Center 1 Research Park Palos Verdes Peninsula, CA 90274 ATTN: Library	1 Copy
Northrop Corporation Electronic Division 2301 120th Street Hawthorne, CA 90250 ATTN: V. Damarting	1 Copy

Physics International Company | 1 Copy each
2700 Merced Street
San Leandro, CA 94577
Attm: C. Stallings
Attn: C. Gilman

R and D Associates | 1 Copy each
P.O. Box 9695
Marina Del Rey, CA 90291
ATTN: W. Graham, Jr.
ATTN: P. Haas

Sandia National Laboratories | 1 copy each
P.O. Box 5800
Albuquerque, New Mexico 87115
ATTN: Doc Con For 3141
ATTN: D. McDaniel
ATTN: P. VanDevender
ATTN: K. Matzen, Code 4247

Science Applications, Inc. | 1 copy
P. O. Box 2351
La Jolla, CA 92038
ATTN: R. Beyster

Spire Corporation | 1 copy
P. O. Box D
Bedford, MA 01730
ATTN: R. Little

SRI International | 1 copy
333 Ravenswood Avenue
Menlo Park, CA 94025
ATTN: S. Dairiki

S-CUBED | 1 copy
P. O. Box 1620
La Jolla, CA 92038
ATTN: A. Wilson

Director
Strategic Defense Initiative Organization | 1 copy each
Pentagon 20301-7100
ATTN: Lt. Col Richard Gullickson/DEO
Dr. Dwight Duston

Texas Tech University | 1 copy
P.O. Box 5404
North College Station
Lubbock, TX 79417
ATTN: T. Simpson

TRW Defense and Space Systems Group | 1 Copy
One Space Park
Redondo Beach, CA 90278
ATTN: Technical Information Center

Vought Corporation | 1 Copy
Michigan Division
38111 Van Dyke Road
Sterling Heights, Maine 48077
ATTN: Technical Information Center
(Formerly LTV Aerospace Corp.)

Naval Research Laboratory
Plasma Radiation Branch
Washington, D.C. 20375

Code 4720 - 50 Copies
Code 4700 - 26 Copies
Code 2628 - 20 Copies

Director of Research
U.S. Naval Academy
Annapolis, MD 21402 | 2 Copies

DATE

ILME